Inorganic Chemistry

Article

pubs.acs.org/IC

$(BiSe)_{1.23}CrSe_2$ and $(BiSe)_{1.22}(Cr_{1.2}Se_2)_2$: Magnetic Anisotropy in the First Structurally Characterized Bi−Se−Cr Ternary Compounds

Samantha M. Clarke and Danna E. Freedman*

Department of Chemistry, Northwestern University, Evanston, Illinois 60208, United States

Supporting Information

ABSTRACT: Compounds containing both heavy main group elements and paramagnetic transition metals form a fertile area for the study of magnetic anisotropy. We pursued the synthesis, characterization, and magnetic measurements of Bi−Se−Cr compounds: a ternary system with no structurally characterized materials. Those efforts led to the isolation of two novel misfit layer compounds, namely, $(BiSe)_{1.23}CrSe_2$ (**1**) and $(BiSe)_{1.22}(Cr_{1.2}Se_2)_2$ (**2**). The crystal structure of **1** consists of alternating BiSe and $CrSe_2$ layers along the *c*-axis, and **2** is composed of alternating BiSe and $(Cr_{1.2}Se_2)_2$ layers along the *c*-axis. Lattice mismatch occurs in both compounds along the *b*-axis and leads to positional modulation of the atoms. Field- and temperature-dependent measurements were performed to assess the degree of magnetic anisotropy. Temperature-dependent susceptibility measurements on aligned crystals of **1** display increased bifurcation of zero-field cooled and field cooled data when crystals are oriented with *H* perpendicular to *c* than when the crystals are oriented with *H* parallel to *c*. Magnetic anisotropy is less pronounced in **2** where both crystallographic orientations exhibit bifurcation at 26 K. The complexity of the magnetic behavior in both compounds likely signifies a competition between $CrSe_2$ intralayer ferromagnetic coupling and interlayer antiferromagnetic coupling. These results highlight the exciting magnetic properties that can arise from the exploration of new ternary phases.

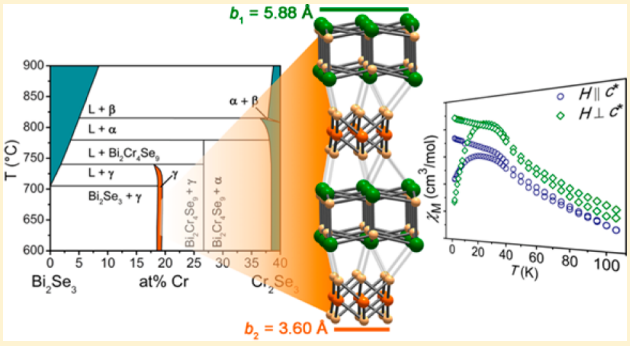

INTRODUCTION

Magnetic anisotropy is both the functional component enabling permanent magnets and the source of various exotic physical properties in materials such as certain topological states.[1] One possible approach to creating magnetic anisotropy is the incorporation of heavy elements into materials, as magnetic anisotropy arises from spin−orbit coupling, which scales with atomic number. While heavy paramagnetic elements such as iridium possess appreciable magnetic anisotropy, our focus is extracting magnetic anisotropy from inexpensive heavy diamagnetic elements, such as bismuth, and combining them with paramagnetic species, such as first-row transition metals. This approach is validated by compounds such as MnBi[2] and the recently discovered $FeBi_2Se_4$,[3] which demonstrate ferromagnetism. Within this general rubric of engendering interactions between paramagnetic species and heavy diamagnetic metals, the underexplored ternary systems of first-row transition metals and bismuth form an excellent area for investigation.

In addition to composition, structure plays a vital role in dictating magnetic properties. The synthesis of low-dimensional structures where the magnetism is primarily confined to a plane offers another mechanism of generating magnetic anisotropy. One such class of compounds are misfit layer chalcogenides, which consist of two interpenetrating two-dimensional (2D) sublattices, MQ and TQ_2 (M = Sn, Sb, Pb, Bi, or a lanthanide, T = Ti, V, Cr, Nb, or Ta, and Q = S, Se, or Te), which are stacked alternately along the crystallographic *c*-axis.[4,5] The in-plane (*a* and *b*) axes are parallel but unequal or incommensurate along one crystallographic direction, which disrupts the periodicity in this direction and causes a structural modulation of the atoms.[6,7] Misfit-layer compounds have attracted interest because of the intriguing properties that originate from structural two-dimensionality. For example, since the degree of structural anisotropy can be varied in these systems, they can elucidate dimensionality aspects of superconductivity.[8]

Within the framework of anisotropic magnetic materials, 2D CrQ_2 sheets are known to show complex magnetic interactions, as demonstrated in $KCrSe_2$,[9] $CuCrSe_2$,[10] and $NaCrSe_2$.[11] While misfit-layer compounds with magnetic CrQ_2 layers have been synthesized,[4,12] only a few of these compounds have been subjected to detailed magnetic characterization. Of these, $LaCrS_3$ is a spin glass due to the modulation of the atoms in the lattice.[13] Another misfit-layer compound, $GdCrS_3$, shows magnetic anisotropy below 30 K as displayed by temperature-dependent susceptibility measurements.[14] As exemplified by these two compounds, simultaneous two-dimensionality and

Received: December 8, 2014
Published: February 23, 2015

DOI: 10.1021/ic5029178
Inorg. Chem. 2015, 54, 2765−2771

lattice mismatch in a magnetic structure can give rise to interesting magnetic properties.

Targeting a low-dimensional system containing bismuth and a transition metal led us to investigate the Bi−Cr−Se ternary system. The exploration of the Bi_2Se_3−Cr_2Se_3 join in 1991 led to preparation of numerous phases, though structural characterization proved elusive.[15] The propensity for bismuth−early transition metal chalcogenides to form misfit-layer structures suggested that the unidentified phases could be misfit-layer compounds. Herein we report the synthesis, structure determination, and magnetic properties of the first structurally characterized bismuth, chromium, and selenium ternary compounds, the misfit-layered species $(BiSe)_{1.23}CrSe_2$ (**1**) and $(BiSe)_{1.22}(Cr_{1.2}Se_2)_2$ (**2**) (Figure 1). These compounds were successfully accessed by crystallization in a eutectic salt flux, which to the best of our knowledge has not been previously employed to crystallize misfit-layer compounds.

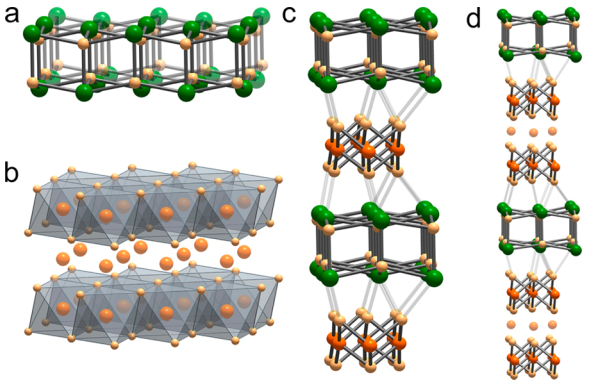

Figure 1. Crystal structures of **1** and **2**. Green spheres represent Bi centers, orange spheres represent Cr centers, and tan spheres represent Se centers. (**a**) BiSe layer depicting rock-salt type structure, viewed down the *a*-axis. (**b**) $(Cr_{1.2}Se_2)_2$ layer of **2** showing octahedral coordination of Cr. (**c**) Average structure of **1** determined from the supercell solution illustrating interlayer bonding. (**d**) Average structure of **2** determined using a supercell. Translucent atoms between paired $CrSe_2$ layers in **b** and **d** indicate partial occupancy of Cr atoms in that layer.

RESULTS AND DISCUSSION

Synthesis. Similar to previously reported misfit-layer compounds, we performed a two-step synthesis of these materials whereby the powdered material was synthesized first by a solid-state reaction and then recrystallized to obtain single crystals suitable for single-crystal X-ray diffraction. Syntheses of $(BiSe)_{1+\delta}CrSe_2$ and $(BiSe)_{1+\delta}(CrSe_2)_2$ were initially pursued through direct combination of stoichiometric quantities of pure elements at 780 °C. However, the reactions failed to produce the desired ternary phases and instead led to the formation of the binaries Bi_2Se_3 and Cr_2Se_3. Therefore, the initial step in the synthesis, the formation of the desired ternary, was achieved by following the Bi_2Se_3−Cr_2Se_3 phase diagram reported in 1991 (Supporting Information, Figure S1).[15] This phase diagram contains two compounds of interest: a compound with the nominal formula $Bi_2Cr_4Se_9$ and a γ-phase with the approximate formula $BiCrSe_3$. Powder patterns of these phases were reported and indexed to unit cells, yet no atomic parameters were obtained.[15] The combination of evidence of compounds with complex structures and constituent elements found in other misfit-layer compounds offered a strong possibility that a misfit-layer compound existed within this region. To access these compounds, as depicted in the phase diagram in Figure S1, the binary precursors Cr_2Se_3 and Bi_2Se_3 were combined in the approximate stoichiometries of the targeted species and heated to 780 °C. Powder X-ray diffraction patterns of the as-synthesized products indicated new phase formation, and the pattern of **2** appears similar to the pattern reported in the literature (Supporting Information, Figure S2).

Following the synthesis of pure product as assessed by a combination of powder X-ray diffraction and elemental analysis, growth of crystals suitable for single-crystal X-ray diffraction was pursued. The most common method of accessing single crystals of misfit-layer compounds is vapor transport with a halogen as a transport agent.[4] Here, we pursued a method not previously employed for the synthesis of misfit-layer compounds: crystallization from a salt flux. Crystallization from a flux is a common synthetic technique, and it has been shown to work for the crystallization of other chalcogenide materials.[16] Here, we employed a LiCl/KCl eutectic salt flux for its advantageously low melting point (352 °C)[17] and compatibility with the constituent elements of **1** and **2**. Salt fluxes also facilitate slow, relatively low-temperature crystallization, which is extremely important for crystallizing layered materials. Crystals of both $(BiSe)_{1.23}CrSe_2$ (**1**) and $(BiSe)_{1.22}(Cr_{1.2}Se_2)_2$ (**2**) appeared as flexible metallic gray sheets from the flux. Control over which misfit-layer compound was produced was achieved by use of the appropriate stoichiometry of the binary starting materials. Crystals of **1** and **2** could be distinguished by powder X-ray diffraction that gave similar but distinct diffraction patterns (Figure S2). The layered nature of these materials leads to the preferential orientation of the crystals along the *c*-axis. This causes the (00*l*) reflections to be well-defined and intense, while *h* or *k* reflections are broad and lower in intensity. Single crystals of each of these compounds were suitable for single-crystal X-ray diffraction, and every form of characterization was performed on single crystals obtained in this manner.

Structure Solution and Description. Synthesis of crystals suitable for single crystal X-ray diffraction enabled structural determination of these two new misfit-layer compounds. To unravel the structure of a misfit-layer material, the structure of each of the two sublattices and their relationship to one another are determined. This was accomplished using diffraction by first solving the structure of each sublattice and then determining the relation between sublattices by solving the structure of an approximate supercell.

The structures of the individual layers were determined from electron and X-ray diffraction data. Initial values for the lattice parameters a, b_1, and b_2 of the two interpenetrating BiSe and $CrSe_2$ sublattices for **1** and **2** were determined by indexing the transmission electron microscope (TEM) selected area electron diffraction (SAED) images and precession images from single-crystal X-ray diffraction (Figures 2 and S3). All other lattice parameters were determined exclusively from single-crystal X-ray diffraction. In both **1** and **2**, the BiSe and $CrSe_2$ subsystems were found to have *C*-centered monoclinic unit cells with the same lattice parameters a, c, and β (Table 1).

Structure solution for each subsystem was performed using reflections exclusive to its unit cell according to previously published methods.[12,18,19] Higher-order common reflections were identified based on the ratio of the *b*-axes, b_2/b_1, which is ~3/5. Specifically, the BiSe subsystem was solved and refined excluding the k = 0, 5 reflections as they are common with the

DOI: 10.1021/ic5029178
Inorg. Chem. 2015, 54, 2765−2771

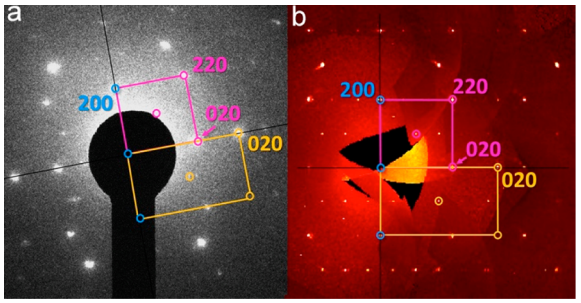

Figure 2. (**a**) SAED image of **2** with incident beam along [001] and (**b**) *hk*1 precession image of **2** showing the presence of two incommensurate lattices. In each image, magenta lines index the BiSe sublattice, and yellow lines index the $CrSe_2$ sublattice, while points circled in blue indicate reflections common to both lattices. See Supporting Information, Figure S3 for corresponding images of **1**.

Table 1. Unit Cell Parameters of Each Sublattice and the Supercells for 1 and 2

chemical formula	$(BiSe)_{1.23}CrSe_2$ (**1**)	$(BiSe)_{1.22}(Cr_{1.2}Se_2)_2$ (**2**)
EDS composition	$(BiSe)_{1.18}Cr_{0.92}Se_{2.2}$	$(BiSe)_{1.11}(Cr_{1.3}Se_2)_2$
BiSe subsystem		
space group	*C*2/*m*	*C*2/*m*
a [Å]	6.1654(18)	6.2060(4)
b_1 [Å]	5.8669(12)	5.8849(5)
c [Å]	11.489(3)	17.2377(10)
β (deg)	95.002(19)	93.552(5)
Z_1	4	4
$R_1{}^a$	12.34%	12.38%
$wR_2{}^b$	30.05%	30.92%
$CrSe_2$ subsystem		
space group	*C*2/*m*	*C*2/*m*
a [Å]	6.1705(11)	6.2049(4)
b_2 [Å]	3.6053(7)	3.5980(3)
c [Å]	11.472(2)	17.2352(12)
β (deg)	95.218(15)	93.535(6)
Z_2	2	2
$R_1{}^a$	13.98%	13.18%
$wR_2{}^b$	36.31%	31.60%
Supercell		
space group	*Cm*	*Cm*
a [Å]	6.1706(19)	6.2044(5)
b_3 [Å]	17.748(5)	17.9594(16)
c [Å]	11.474(4)	17.2313(15)
β (deg)	95.04(3)	93.537(7)
Z_3	8	8
$R_1{}^a$	14.75%	11.79%
$wR_2{}^b$	31.02%	33.90%

$^aR_1 = \sum||F_0| - |F_c||/\sum|F_0|$ $^bwR_2 = [\sum[w(F_0^2 - F_c^2)^2]/\sum[w(F_0^2)^2]]^{1/2}$

$CrSe_2$ part, while the $CrSe_2$ subsystem was solved excluding reflections with $k = 0, 3$. For each compound, the unit cell of each sublattice was integrated separately in the APEX2 software package followed by solution and refinement using Shelx with the Olex2 interface.[20,21]

Following structure determination of each sublattice, the relationship between the two layers was established. Because of the incommensurate character along *b*, it is impossible to relate the *x*- and *z*-coordinates of both parts using the lattice parameters of either sublattice with this solution method. Therefore, the relative *x* and *z* positions of the BiSe and $CrSe_2$ sublattices in **1** and **2** were resolved by approximating the structure to a supercell. The lattice parameters b_1 of the BiSe layer and b_2 of the $CrSe_2$ layer give the approximate ratios $b_2/b_1 = 0.6145$ for **1** and $b_2/b_1 = 0.6113$ for **2**. The ratios are irrational, indicating that the compounds are incommensurately modulated. However, since the ratios are sufficiently close to 3/5, an approximate supercell can be derived to allow for the determination of the positions of the layers with respect to one another. The selected supercell shares similar *a*, *c*, and *β*, parameters to the $CrSe_2$ and BiSe layers, while the b_3 parameter is approximately 3 times b_1 and 5 times b_2. Within the general formula for a misfit-layer chalcogenide $(MQ)_{1+\delta}(TQ_2)_n$ the parameter δ can take any value between 0.8 and 0.28.[4] The value of δ is calculated from $\delta = (Z_1/Z_2)(b_2/b_1) - 1$, where *Z* is the number of chemical formula units per unit cell (Table 1) and yields values of $\delta = 1.23$ and $\delta = 1.22$ for **1** and **2**, respectively.[4] The final structures of both compounds, depicted in Figure 1, illustrate the individual layers and their interaction.

The final structure of **1** consists of rock-salt type BiSe layers and edge-sharing octahedral $CrSe_2$ layers (Figure 1). The Bi atoms in the BiSe layer are bonded to five Se atoms within that same layer and two Se atoms from the $CrSe_2$ layer. The intralayer bonds between Bi and Se range from ∼2.8 Å to ∼3.3 Å, compared to the interlayer bonds, which range from ∼3.0 to ∼3.4 Å (see Supporting Information CIF for detailed distances). The ranges are comparable to that of Bi_2Se_3 (2.819(3) to 3.545(3) Å).[22] The average structure for **1** shows the BiSe and $CrSe_2$ layers alternate in a 1:1 ratio along the *c*-axis (Figure 1c), yielding the complete empirical molecular formula of $(BiSe)_{1.23}CrSe_2$. Assignment of a formal oxidation state of +3 for Bi and Cr and −2 for Se leads to an overall charge of +0.23 for the unit cell. The residual positive charge could be compensated by Bi vacancies present in the structure or a lower than 3+ oxidation state for Bi, both of which have been observed in other misfit-layer compounds.[14,23] The assigned oxidation states are consistent with our data from X-ray photoelectron spectroscopic results, as detailed in the Supporting Information. The stability of the interlayer Bi−Se bonds and the lattice mismatch along the *b*-direction induces a positional modulation of the atoms, which is partially responsible for the nonideal refinement statistics. The slightly longer interlayer bond lengths suggest a weaker bonding interaction than the intralayer bonds.

Elemental analysis of **1** via scanning electron microscopy energy dispersive X-ray spectroscopy (SEM-EDS) revealed 21.6(5) % Bi, 16.9(5) % Cr, and 61.6(1) % Se. These values deviate by less than 2% from those expected from the crystal structure supporting the crystallographically obtained empirical formula. Notably no evidence is given in the EDS spectra of other elements present in the crystal.

The bonding of misfit-layer compound **2** is very similar to that of **1**. For example, the Bi atoms of the BiSe layer are bound to five Se atoms within that same layer and two Se atoms from the neighboring $CrSe_2$ layer. Intralayer bonds between Bi and Se range from ∼2.75 to ∼3.2 Å, compared to the interlayer bonds which range from ∼3.1 to ∼3.4 Å, similar to those found in **1** and pure Bi_2Se_3.[22] As in **1**, the interlayer bonds of **2** coupled with the misfit along the *b*-axis cause positional modulation of the atoms resulting in large refinement statistics for the solution. The primary structural difference between **1** and **2** is for each BiSe layer there are two complete $CrSe_2$ layers in **2** (Figure 1d). Typically, in double-layer misfit compounds, there is a van der Waals gap between paired TX_2 layers.[4,5] However, in this system, the refinement indicates partial

DOI: 10.1021/ic5029178
Inorg. Chem. 2015, 54, 2765−2771

occupancy of sites within the assumed van der Waals layer, which we expect to be Cr centers. This is supported by the fact that no other elements are detected in the EDS spectra. An occupation of ~0.44 Cr was found from the refinement. Partial occupation of the van der Waals gap has been observed in other paired TX_2 misfit-layer compounds such as $PbNb_2S_5$.[18] The excess Cr in the octahedral sites between paired $CrSe_2$ layers is consistent with charge balance for this compound. Assigning a formal oxidation state of +3 for Bi and Cr and −2 for Se yields an overall charge of −0.8 without Cr in the van der Waals positions and +0.4 with the Cr. Thus, the excess Cr centers appear to assist in stabilizing charges within the compound. Similar to **1** and other misfit-layer compounds, the excess positive charge may be from Bi vacancies or a lower than 3+ oxidation state for Bi.[14,23] The empirical molecular formula determined from the solution of each sublattice was found to be $(BiSe)_{1.22}(Cr_{1.2}Se_2)_2$ for **2**.

Elemental analysis via SEM-EDS was performed to verify the stoichiometry determined from the crystal structure. The atomic percentages of the elements are 12.5(6) % Bi, 29.3(5) % Cr, and 58.2(1) % Se. The percentage of selenium matches very well to that which is expected from the crystal structure, and those of bismuth and chromium deviate by less than 2%. As discussed above, this discrepancy could be attributed to the presence of bismuth vacancies to balance the charge. Importantly, there is no evidence of other elements in the EDS spectrum. The agreement between the chemical formula obtained from diffraction and elemental analysis demonstrates the empirical formula of compound **2** is $(BiSe)_{1.22}(Cr_{1.2}Se_2)_2$ and provides additional evidence the structural solution is accurate.

Magnetic Measurements. Magnetometry data were acquired to ascertain the degree of magnetic anisotropy present within these two compounds. All data were collected on a stack of oriented single crystals of **1** and **2**. To fully magnetically characterize these samples, a combination of direct current (dc) magnetic susceptibility and alternating current (ac) magnetic susceptibility measurements were performed. The temperature-dependent magnetic susceptibility data offer insight into the magnetic coupling between paramagnetic Cr^{3+} centers; ac susceptibility data ascertain the nature of any ordering transition. The aggregate of these data create a thorough picture of the magnetic behavior of **1** and **2**.

Magnetic susceptibility (χ_M) data were acquired on **1** under an applied dc magnetic field of H_{dc} = 1 T (Figure 3a). In the temperature range of 250 to 34 K, χ_M increases monotonically from 0.0090 to 0.0139 cm^3/mol for crystals with $H\|c$ and from 0.0094 to 0.0151 cm^3/mol for crystals with $H\perp c$. A bifurcation between the zero-field cooled (ZFC) and field cooled (FC) data in **1** is observed below 34 K indicating a magnetic transition below this temperature. As indicated in Figure 3a, the bifurcation takes the common form where the ZFC data display a downturn in susceptibility with decreasing temperature, while the FC data show an upturn. The divergence of these curves indicates the freezing of the magnetic moments in a disordered state when cooled in zero applied dc field. With increasing temperature, the influx of energy provides trapped moments with enough energy to overcome any existing energy barrier to realignment. The moments then either align with the field or along a preferred crystallographic direction. The broadness of the transition temperature offers insight into the nature of the phenomenon. It can likely be attributed to the two-dimensionality of the system, since in higher dimensional

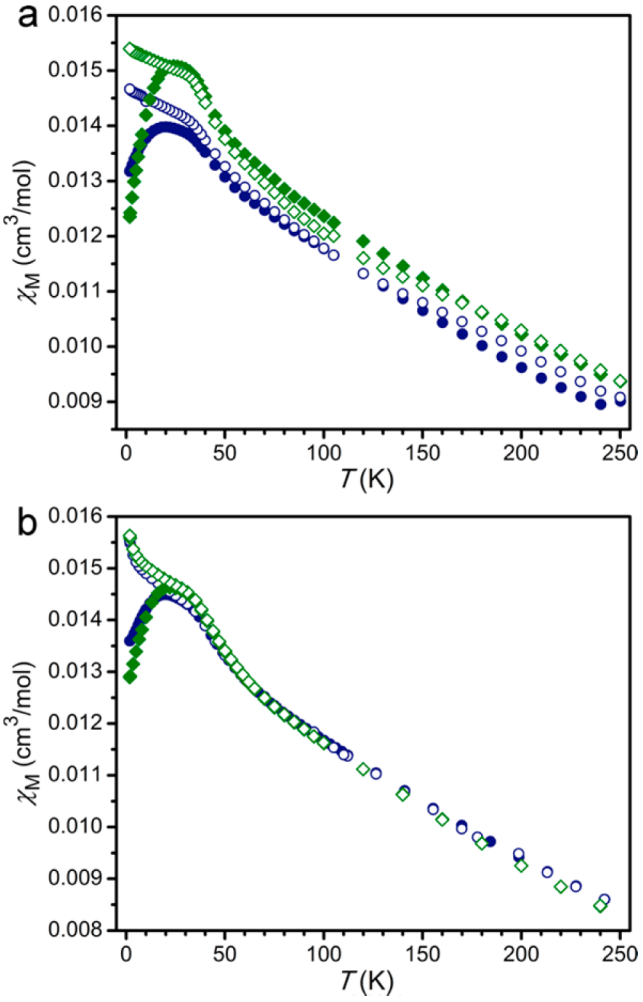

Figure 3. Variable-temperature molar dc magnetic susceptibility of oriented single crystals of **1** (**a**) and for **2** (**b**) with H_{dc} = 1 T. Green ◆ indicate $H\perp c$, and blue ● indicate $H\|c$. Filled shapes indicate ZFC measurement, and outlined shapes indicate FC measurement.

systems, greater cooperativity between spin centers leads to sharper magnetic transitions. However, the broadness could also be attributed to competing interactions between different magnetic coupling pathways. The susceptibility of crystals of **1** with $H\perp c$ reaches 0.0154 cm^3/mol at 1.8 K, 0.0007 cm^3/mol larger than what is observed at that temperature for the opposite orientation, indicating the *ab* plane as an easy plane of magnetization. Additionally, the bifurcation of the ZFC and FC data is much more pronounced in this orientation, differing by 0.0031 cm^3/mol at 1.8 K, versus the 0.0015 cm^3/mol difference at the same temperature observed for the crystals oriented with $H\|c$.

The susceptibility data above 90 K for crystals with $H\perp c$ was fit to the Curie–Weiss law, $\chi = C/(T - \theta)$, yielding C = 5.80(3) cm^3 K/mol, θ = −367(3) K, and an effective magnetic moment of μ_{eff} = 6.79 μ_B (Supporting Information, Figure S6). The μ_{eff} is anomalously larger than the value expected for that of Cr^{3+} ($S = {}^3/_2$, g = 2.00, μ_{eff} = 3.87 μ_B). This value was consistent over multiple samples and repeated measurements. We hypothesize that this indicates the high-temperature data are not in the paramagnetic regime up to 250 K. Similar explanations have been offered for this behavior in the $CrSe_2$ layers of $CuCrSe_2$.[10] In this case, the obtained values of C and θ

DOI: 10.1021/ic5029178
Inorg. Chem. 2015, 54, 2765−2771

do not have significance since the equation is not valid under those conditions. The Curie–Weiss fit for crystals oriented with $H||c$ does not significantly differ from that obtained with $H\perp c$.

The magnetic data of **2** (Figure 3b) are similar to those of **1** but demonstrate fewer characteristics of magnetic anisotropy. From 250 to 26 K and H_{dc} = 1 T, the χ_M value of **2** increases monotonically from 0.008 to 0.014 cm^3/mol for both $H||c$ and $H\perp c$. Below 26 K, the ZFC and FC curves bifurcate as was also observed in **1** and likely for the same reason. However, the magnitude of the splitting is only slightly different between orientations, where the crystals oriented with $H\perp c$ split 0.0008 cm^3/mol more than crystals with $H||c$. The susceptibility data above 90 K for crystals with $H\perp c$ were fit to the Curie–Weiss law giving C = 4.25(6) cm^3 K/mol and θ = −263(7) K (Figure S6). Normalizing the Curie constant per mole of Cr yields C = 1.78 cm^3 K/mol and μ_{eff} = 3.76 μ_B, which in contrast to **1** is consistent with the expected value for Cr^{3+} (μ_{eff} = 3.87 μ_B). However, the similarity between the compounds prevents us from confirming this compound is within the paramagnetic regime suitable for the use of the Curie–Weiss equation.

The observation of the bifurcation of ZFC and FC data for **1** and **2** highlights the complex magnetic interactions in these materials. The Goodenough–Kanamori rules[24,25] allow for the prediction of the sign of exchange coupling between paramagnetic transition metal ions through a bridging diamagnetic ligand, such as selenium, as a function of local geometry.[26] For two Cr^{3+} ions ($3d^3$) bridged by Se^{2-} ions, a Cr–Se–Cr angle at or close to 90°, as occurs in the $CrSe_2$ layers of **1** and **2**, typically generates a ferromagnetic Cr···Cr interaction, which engenders ferromagnetic ordering. Additionally, the strong increase in the FC magnetization below the transition temperature in each compound indicates increasing influence of ferromagnetic interactions. However, the absence of a sharp peak in the out-of-phase ac susceptibility data and the broad nature of the transition are more indicative of lower-dimensional magnetic behavior. In addition, the large extrapolated Curie–Weiss parameters for **1** and **2** indicate strong antiferromagnetic interactions in both compounds, which we attribute to antiferromagnetic coupling between $CrSe_2$ layers. However, the magnitude of these parameters must be evaluated with skepticism since the data being fit may be outside of the paramagnetic regime where the Curie–Weiss law is applicable.

The complex magnetic behavior of these misfit-layer compounds is indicative of competing intra- and interlayer magnetic interactions. A broad transition temperature and bifurcation of the ZFC and FC curves has been observed in other layered materials including the spin glass $LaCrS_3$.[10,11,13] However, no peaks were observed in variable-temperature ac susceptibility data in either the in-phase or out-of-phase region from 3 to 200 K at ac fields of 100 and 1000 Hz (Figures S6 and S7). Note, the characteristic ac susceptibility behavior of a spin glass was observed in $LaCrS_3$. Thus, at this stage assignment of spin-glass behavior cannot be sustained, although the possibility of a spin-glass transition spread out over a large temperature range cannot be excluded by the data. Such a large transition range could be mediated by the Bi defects in the material allowing several different local transition temperatures.

Given the similar atomic structures of the magnetic $CrSe_2$ layers in **1** and **2**, a difference in magnetic anisotropy between the two compounds is notable. One possibility for the difference is greater interaction between the bismuth centers and the chromium centers in **1**. In **2**, only the exterior layers of the $CrSe_2$ sublattice are in contact with bismuth. An alternate hypothesis would be the more 2D nature of the $CrSe_2$ component of **1**. Future research will focus on studying structural analogues including other chromium misfit-layer compounds with heavy metals such as Sn, Sb, and Pb to gain insight into the magnetic differences between these two compounds. Single-crystal transport measurements will also serve to elucidate the structure–function relationship.

CONCLUSIONS AND OUTLOOK

The foregoing results illustrate the synthesis and characterization of the first structurally characterized Bi–Cr–Se ternary compounds, $(BiSe)_{1.23}CrSe_2$ and $(BiSe)_{1.22}(Cr_{1.2}Se_2)_2$. They were shown, by a combination of single-crystal X-ray diffraction and electron diffraction, to be misfit-layer compounds with incommensurability along the b-axes. Notably, the structural anisotropy is posited to play a large role in the dictating the overall magnetic anisotropy of the two compounds, as evidenced by the results of magnetic measurements on aligned single crystals. Irreversibility in temperature-dependent dc magnetization under field cooling suggests either ferromagnetism or spin-glass freezing; however, the lack of features in the out-of-phase ac susceptibility demonstrates the need for further study. Our future investigations on these materials will expand the properties under investigation to other phenomena that may be strongly affected by the 2D structure, such as electronic transport properties. Further, intercalation of different ions into the van der Waals gap of the double-layer compound may generate new electronic or magnetic properties.

EXPERIMENTAL DETAILS

Synthesis. All manipulations were performed under a dinitrogen atmosphere unless otherwise specified. Metal reagents were all purchased from commercial vendors: Bi pieces (Rotometals 99.99 %), Cr powder (Alfa Aesar 99 %), and Se powder (Alfa Aesar 99+ %). Samples were synthesized by direct combination of binaries followed by flux crystallization. Binary precursor compounds Bi_2Se_3 and Cr_2Se_3 were synthesized by combining stoichiometric amounts of the elements in fused-silica tubes and heating to 750 °C for Bi_2Se_3 and to 1000 °C for Cr_2Se_3, holding there for 3 d, then cooling to room temperature over an hour. Purity of the precursors was confirmed by powder X-ray diffraction. Synthesis of microcrystalline $(BiSe)_{1.23}CrSe_2$ (**1**) was performed by combining Bi_2Se_3 (1.05 g, 1.6 mmol) and Cr_2Se_3 (0.45 g, 1.3 mmol) in sealed carbon-coated fused-silica tubes under vacuum. Synthesis of microcrystalline $(BiSe)_{1.22}(Cr_{1.2}Se_2)_2$ (**2**) was performed by combining Bi_2Se_3 (1.47 g, 2.24 mmol) and Cr_2Se_3 (1.53 g, 4.49 mmol) in sealed carbon-coated fused-silica tubes under vacuum. The tubes were heated to 780 °C at a constant rate of 48.7 °C/h over 15 h. The temperature was maintained for 165 h at 780 °C, and then the samples were slowly cooled at a rate of 13.3 °C/h to 180 °C over 45 h. Finally, the furnace was turned off, and the samples were left to cool to room temperature. For both syntheses, the resulting powders were removed from the tubes, ground, and characterized by powder X-ray diffraction. All grinding was performed under an anaerobic atmosphere. The annealing process described above was repeated twice more to obtain higher yields of the products. Preparation of phase-pure single crystals occurred through crystallization in a salt flux, where 0.4 g of each sample was combined with KCl (0.84 g, 11.1 mmol) and LiCl (1.16 g, 27.4 mmol) in sealed carbon-coated fused-silica tubes under vacuum. The tubes were heated to 780 °C at a rate of 48.7 °C/h and subsequently slowly cooled to 355 °C at a rate of 1.7 °C/h, at which point the oven was turned off, and the tubes were left to cool to room temperature. The tubes were opened to air, and the salt matrix was dissolved in distilled water. The product consisted of a combination of microcrystalline powder and shiny, platelike crystals with dimensions of up to 0.02 × 1 × 1 mm^3.

DOI: 10.1021/ic5029178
Inorg. Chem. 2015, 54, 2765–2771

X-ray Diffraction. All compounds were characterized by powder X-ray diffraction with Cu Kα (λ = 1.541 78 Å) radiation on a PANalytical Empyrean diffractometer with a PIXcel 1D detector. Single-crystal X-ray diffraction for **1** was performed at 250 K on a Bruker Kappa APEX2 diffractometer with a Mo Kα (λ = 0.710 73 Å) sealed tube source and Triumph monochromator. Data collection for **2** was performed at 250 K on a Bruker Kappa APEX2 diffractometer with a Cu Kα IμS microfocus source with MX Optics. Data collection, cell refinement, data reduction, and generation of procession images were carried out using the program APEX2.[20] Numerical absorption corrections were performed with the program SADABS.[20,21] Structure solution and refinement was performed using the SHELXTL package with the Olex2 software interface.[21] Additional solution details and refinement results for **1** and **2** can be found in the Supporting Information.

Electron Microscopy. Transmission electron microscopy (TEM) was performed on a Hitachi HT-7700 TEM with 100 kV accelerating voltage. Selected area electron diffraction (SAED) images were collected with a CCD camera. Samples were prepared by suspending small crystals in isopropanol, placing a small amount of suspension on a copper grid, and allowing it to dry in air. Scanning electron microscopy (SEM) was performed on a Hitachi S-3400N−II using a 25 kV electron beam. An Oxford INCAx-act SSD EDS was used to perform energy-dispersive X-ray spectroscopy (EDS) to determine elemental composition. Ten different points per crystal were taken. Samples were mounted on conductive carbon tape on aluminum stages.

Magnetic Measurements. All magnetic data were collected on a Quantum Design MPMS-XL at a temperature range of 1.8 to 250 K and under applied dc fields ranging from 0 to 7 T. Oriented crystalline samples were prepared by affixing single crystals to the end of a quartz rod using paratone oil for **1** and Duco cement for **2**. Further details of magnetic characterization can be found in the Supporting Information.

■ ASSOCIATED CONTENT

Supporting Information

Additional synthetic details; note on ternary compounds; X-ray powder diffraction; further discussion of the methods used to solve the crystal structure; X-ray photoelectron spectroscopy data; additional magnetic information; magnetic susceptibility data; tables of crystallographic data; crystal structures in the form of CIF files; additional references. This material is available free of charge via the Internet at http://pubs.acs.org.

■ AUTHOR INFORMATION

Corresponding Author

*E-mail: danna.freedman@northwestern.edu.

Author Contributions

All authors have given approval to the final version of the manuscript.

Funding

This work was supported by the MRSEC program of the National Science Foundation (DMR-1121262) at the Materials Research Center of Northwestern Univ. This work made use of the EPIC facility (NU*ANCE* Center-Northwestern Univ.), which has received support from the MRSEC program (NSF DMR-1121262) at the Materials Research Center; the Nanoscale Science and Engineering Center (NSF EEC−0647560) at the International Institute for Nanotechnology; and the State of Illinois, through the International Institute for Nanotechnology. This work made use of the IMSERC X-ray facilities funded by the State of Illinois. This XPS work was performed in the Keck-II facility of NU*ANCE* Center at Northwestern Univ. The NU*ANCE* Center is supported by NSEC (NSF EEC-0647560), MRSEC (NSF DMR-1121262), the Keck Foundation, the State of Illinois, and Northwestern Univ.

Notes

The authors declare no competing financial interest.

■ ACKNOWLEDGMENTS

The authors thank Dr. A. Sarjeant, Ms. C. Stern, Prof. D. Fredrickson, Dr. D. Gray, and Dr. C. Malliakas for their crystallography assistance and Mr. A. Mouat, Mr. N. Calta, and Dr. J. Zadrozny for experimental assistance and helpful discussion.

■ REFERENCES

(1) (a) Kirchmayr, H. R. *J. Phys. D: Appl. Phys.* **1996**, *29*, 2763−2778. (b) Herbst, J. F.; Croat, J. J.; Pinkerton, F. E.; Yelon, W. B. *Phys. Rev. B* **1984**, *29*, 4176−4178. (c) Tang, E.; Mei, J.-W.; Wen, X.-G. *Phys. Rev. Lett.* **2011**, *106*, 236802.

(2) Adams, E.; Hubbard, W. M.; Syeles, A. M. *J. Appl. Phys.* **1952**, *23*, 1207−1211.

(3) Ranmohotti, K. G. S.; Djieutedjeu, H.; Lopez, J.; Page, A.; Haldolaarachchige, N.; Chi, H.; Sahoo, P.; Uher, C.; Young, D.; Poudeu, P. F. P. *J. Am. Chem. Soc.* **2015**, *137*, 691−698.

(4) Wiegers, G. A. *Prog. Solid State Chem.* **1996**, *24*, 1−139.

(5) Rouxel, J.; Meerschaut, A. *Mol. Cryst. Liq. Cryst.* **1994**, *244*, 343−354.

(6) Jobst, A.; van Smaalen, S. *Acta Crystallogr., Sect. B: Struct. Sci.* **2002**, *58*, 179−190.

(7) Onoda, M.; Kato, K.; Gotoh, Y.; Oosawa, Y. *Acta Crystallogr., Sect. B: Struct. Sci.* **1990**, *46*, 487−492.

(8) (a) Van Maaren, M. H. *Phys. Lett. A* **1972**, *40*, 353−354. (b) Schmidt, L. *Phys. Lett. A* **1970**, *31*, 551−552. (c) Reefman, D.; Koorevaar, P.; Brom, H. B. *Synth. Met.* **1991**, *41−43*, 3775−3780. (d) Nader, A.; Briggs, A.; Meerschaut, A.; Lafond, A. *Solid State Commun.* **1997**, *102*, 401−403.

(9) Fang, C. M.; Tolsma, P. R.; van Bruggen, C. F.; de Groot, R. A.; Wiegers, G. A.; Haas, C. *J. Phys.: Condens. Matter* **1996**, *8*, 4381−4388.

(10) Tewari, G. C.; Karppinen, M.; Rastogi, A. K. *J. Solid State Chem.* **2013**, *198*, 108−113.

(11) Engelsman, F. M. R.; Wiegers, G. A.; Jellinek, F.; van Laar, B. *J. Solid State Chem.* **1973**, *6*, 574−582.

(12) Lafond, A.; Fragnaud, P.; Evain, M.; Meerschaut, A. *Mater. Res. Bull.* **1992**, *27*, 705−713.

(13) Lafond, A.; Meerschaut, A.; Rouxel, J.; Tholence, J. L.; Sulpice, A. *Phys. Rev. B* **1995**, *52*, 1112−1119.

(14) Rouxel, J.; Moëlo, Y.; Lafond, A.; Disalvo, F. J.; Meerschaut, A.; Roesky, R. *Inorg. Chem.* **1994**, *33*, 3358−3363.

(15) Shabunina, G. G.; Kireeva, E. V.; Aminov, T. G. *Russ. J. Inorg. Chem.* **1996**, *41*, 1496−1498.

(16) Liu, X.; Fechler, N.; Antonietti, M. *Chem. Soc. Rev.* **2013**, *42*, 8237−8265.

(17) Basin, A. S.; Kaplun, A. B.; Meshalkin, A. B.; Uvarov, N. F. *Russ. J. Inorg. Chem.* **2008**, *53*, 1509−1511.

(18) Auriel, C.; Meerschaut, A.; Rouxel, J.; Nantes, U. De. *Mater. Res. Bull.* **1993**, *28*, 675−684.

(19) Laond, A.; Deudon, C.; Meerschaut, A.; Palvadeau, P.; Moëlo, Y.; Briggs, A. *J. Solid State Chem.* **1999**, *142*, 461−469.

(20) Bruker. *APEX2,* Version 2009.5−1: Data Collection and Processing Software; Bruker Analytical X-Ray Instruments, Inc.: Madison, WI, 2009.

(21) Sheldrick, G. M. *Department of Structural Chemistry;* University of Göttingen: Göttingen, Germany, 2008.

(22) Atabaeva, E. Y.; Mashkov, S. A.; Popova, S. V. *Krystallografiya* **1973**, *18*, 173−174.

(23) Ettema, A. R. H. F.; Haas, C. *J. Phys.: Condens. Matter* **1993**, *5*, 3817−3826.

(24) Goodenough, J. B. *J. Phys. Chem. Solids* **1958**, *6*, 287−297.

(25) Kanamori, J. *J. Phys. Chem. Solids* **1959**, *10*, 87−98.

DOI: 10.1021/ic5029178
Inorg. Chem. 2015, 54, 2765−2771

(26) (a) Poudeu, P. F. P.; Takas, N.; Anglin, C.; Eastwood, J.; Rivera, A. *J. Am. Chem. Soc.* **2010**, *132*, 5751−5760. (b) Bensch, W.; Sander, B.; Kremer, R. K.; Kockelmann, W. *J. Solid State Chem.* **2001**, *158*, 198−207.

DOI: 10.1021/ic5029178
Inorg. Chem. 2015, 54, 2765−2771